Micromagnetic investigation of a voltage-controlled skyrmionic magnon switch

Zedong Hu[1,*], Yixin Shao[1], Victor Lopez-Dominguez[1], Pedram Khalili Amiri[1,*]

[1] Department of Electrical and Computer Engineering, Northwestern University, Evanston, IL, USA

* e-mail: zedonghu2021@u.northwestern.edu, pedram@northwestern.edu

Abstract

This work proposes and numerically studies a skyrmionic magnon switch (SMS) device, where a Néel-type skyrmion acts as a programmable scattering center to route propagating spin waves. Our results show that the effective deflection of magnons by a skyrmion strongly depends on the ratio of magnon wavelength to skyrmion diameter, being as large as 30° when the skyrmion diameter is comparable with the magnon wavelength. This offers the possibility to program the routing of magnons in a network of ferromagnetic wires, by controlling the perpendicular magnetic anisotropy (PMA) of the ferromagnetic film via the voltage-controlled magnetic anisotropy effect (VCMA), which in turn controls the skyrmion size, stability, and the spin wave deflection angle. The proposed SMS device allows for electrical routing of spin waves between branches of a magnonic circuit, a functionality that is fundamental to emerging magnonic logic and computing concepts. It is shown that on/off ratios as large as 90× are achievable in such an SMS device using realistic material parameters.

I. INTRODUCTION

Collective excitations of the magnetization in ferromagnets, known as spin waves or magnons, have been proposed to encode and carry information in magnonic computing (MC) circuits [1-5]. Magnonic computing offers a number of advantages over conventional charge-based computing, including low power dissipation (since magnon propagation does not require charge transfer), and reduced component count of certain classical logic operations (e.g. majority gates), due to the fact that information can be encoded both in the amplitude and the phase of the spin wave [4,6-9]. This has resulted in increased interest in MC, particularly for special-purpose magnonic co-processors that could be deployed alongside conventional digital logic circuits, to accelerate certain computational tasks such as pattern and speech recognition [5,10,11]. At the same time, with the accelerated development of quantum computing systems, magnons have emerged as potential information carriers on quantum interconnects and as intermediate particles for quantum frequency transduction, both of which play important roles in scaling quantum systems to large numbers of interconnected qubits [12-15]. One of the challenges in the realization of most MC concepts, however, is that they require an efficient and reconfigurable approach for routing spin waves in complex networks of magnetic wires [4,16-21]. Here we propose to utilize interactions of propagating spin waves with magnetic Néel-type skyrmions to address this challenge.

Skyrmions are topologically protected textures of the magnetization in a magnetic material [22]. Their observation and manipulation in systems with bulk Dzyaloshinskii-Moriya interaction (b-DMI) such as chiral ferromagnets [23], and especially in heavy metal/ferromagnetic heterostructures [24-26] with interfacial Dzyaloshinskii-Moriya interaction (i-DMI), have given rise to numerous proposals for skyrmion-based device applications. For example, it has been proposed to use the presence or absence of skyrmions to encode digital information along a magnetic wire [27,28], where skyrmions can be moved by spin-orbit torques and read out electrically, e.g. via the tunnel magnetoresistance (TMR) effect [29]. Room-temperature electrical skyrmion nucleation, motion, and control via an electric field have all recently been demonstrated

in i-DMI systems [24,30-32].

Here, we go beyond this skyrmion-based data storage paradigm, and propose to use electrically-controlled skyrmions not just as nonvolatile memory elements, but as programmable elements for routing magnons in ferromagnetic waveguides. This combination provides a platform for combined magnonic logic and topologically protected nonvolatile memory operation in a single skyrmionic magnon switch (SMS) device. Recent numerical and theoretical studies have shown that low-energy short-wavelength spin waves can induce resonant rotation and breathing modes in a skyrmion [33], while larger spin wave energies may also allow for momentum transfer by the spin waves to the skyrmion, resulting in skyrmion motion without charge currents [29,34,35]. Here we focus on magnons with intermediate energies and wavelengths, where a rigid interaction mode is expected. In this case, the skyrmion acts as a scattering center for the spin wave, without significant deformation of the skyrmion [36-39]. In addition, an electric field is used to tune both the magnon wavelength and the skyrmion diameter, thus allowing for voltage-tunable scattering of magnons by skyrmions.

The paper is organized as follows. In Section II.A, we perform a systematic micromagnetic study of the interaction between exchange spin waves and skyrmions stabilized by i-DMI in a thin ferromagnetic wire. First, we study the dependence of the skyrmion diameter and spin wave dispersion on i-DMI and PMA in a ferromagnetic wire with perpendicular magnetization in contact with a heavy metal, using material parameters similar to previous experiments in Pt/Co and Ta/CoFeB material systems. Then, we study the magnon deflection due to the presence of a skyrmion in the magnetic wire, and demonstrate a method to control the deflection electrically, where the magnetic anisotropy is modified by a voltage via the voltage-controlled magnetic anisotropy (VCMA) effect [40-44]. In Section II.B, we then investigate the proposed skyrmionic magnon switch device, where spin waves are effectively routed by a skyrmion placed at the intersection of two ferromagnetic wires (i.e. magnonic waveguides). We show that the on/off ratio of this SMS device is affected by the presence of edge mode spin waves and depends on the magnetic wire widths. An on/off ratio as large as 90× is demonstrated.

II. RESULTS AND DISCUSSION

A. Spin wave - skyrmion interactions in a ferromagnetic wire

All simulations in this work were performed using the open-source micromagnetic simulation package mumax^3 [45,46]. The magnonic waveguides consisted of a ferromagnetic film with thickness of 1 nm, patterned into a wire geometry with lateral width of 200 nm and length of 4000 nm. Other details of the structure are shown in Fig. 1(a), including the skyrmion position which is shown as a black circle. To reduce the spin wave reflection from the waveguide termination, we applied an increased damping coefficient at the end of the wire, which is shown in dark gray color in Fig. 1(a) [47,48] and is marked as the "damping region". We considered typical material parameters for thin metallic ferromagnetic films, specifically a saturation magnetization, M_s, of 580 kA m^{-1} along the z direction (due to the perpendicular magnetic anisotropy), exchange constant A of 15 pJ m^{-1}, and a damping constant of 0.01 [49].

To investigate the skyrmion stability, a skyrmion was manually initialized by locally flipping the magnetization in a region of the magnetic wire, followed by allowing the magnetization to relax to an equilibrium configuration over a time period of 10 ns. The resulting diameter of the stable skyrmion, d, was studied as a function of the i-DMI, D, and PMA, K_u, coefficients, as shown in Fig. 1(b). The results indicate that higher i-DMI increases the skyrmion diameter, while an increase of the anisotropy constant reduces the skyrmion diameter. Note that higher PMA constants also make it possible to have a stable skyrmion over a wider range of i-DMI values. We note that these results are in good agreement with previous studies on skyrmion stability in similar material systems [49].

Before studying the skyrmion-spin wave interaction, we separately simulated the spin wave spectrum in the above-described magnetic wire in the absence of a skyrmion. Spin waves were excited by a sinusoidal magnetic field, $\boldsymbol{h} = \boldsymbol{x}hsin(2\pi ft)$, where h denotes the amplitude of the field (always being 1 mT), f is the field frequency, t is the simulation time, and $\boldsymbol{x}$ is the unit vector along the axis parallel to the wire length. This ac field was applied in a 6 nm wide region, as shown in Fig. 1(a), to mimic the operation

of an inductive antenna patterned on top of the wire. The results are shown in Fig. 1(c), indicating an exchange spin wave mode [8,50,51] excited by this sinusoidal field. The simulated dispersion is in excellent agreement with analytical results.

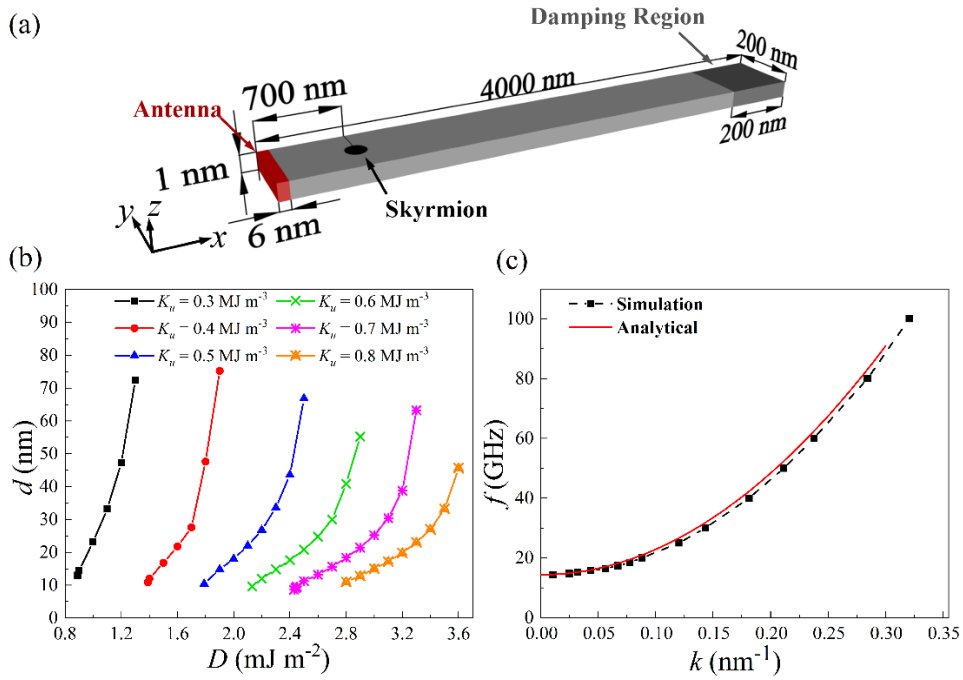

FIG 1. (a) Structure of the magnetic wire used in our simulations. Red and black areas represent the antenna region (used to excite the spin waves) and the skyrmion, respectively. To reduce spin wave reflection from the right end of the wire, the damping coefficient in the dark gray highlighted "damping region" was gradually increased from 0.01 to 1.00 over the distance 3800 nm $\leq l \leq$ 4000 nm, where l is the distance from the left edge of the wire; (b) Dependence of skyrmion diameter (d) on the i-DMI coefficient (D), for different values of the perpendicular magnetic anisotropy (K_u) varying from 0.3 to 0.8 MJ m^{-3}. The equilibrium skyrmion diameter grows with increasing i-DMI values and decreases as PMA increases. (c) Dispersion curve of exchange spin waves excited by the ac magnetic field in the antenna region. The solid red curve shows the analytical solution of exchange magnons and is in good agreement with the numerical results. This curve is given by $\omega_{ex} = \gamma H_{eff} + A/K_u \cdot \gamma M_s k^2$, where γ is the gyromagnetic ratio, H_{eff} is the effective magnetic field ($H_{eff} = 2\,K_u/(\mu_0 M_s) - M_s$), A is the exchange stiffness, M_s is the saturation magnetization, and K_u is the perpendicular magnetic anisotropy coefficient, which depends on voltage due to the VCMA effect. The material parameters are the same as those used for the skyrmion simulations, M_s = 580 kA m^{-1}, D = 1.7 mJ m^{-2}, A = 15 pJ m^{-1}, and K_u = 0.36 MJ m^{-3}.

We next turned our attention to simulating spin wave propagation and scattering in the presence of a skyrmion. Figure 2 shows the dependence of the spin wave deflection angle θ as a function of the ratio of the magnon wavelength to skyrmion diameter ($R = \lambda/d$), based on simulations of several cases with different magnon wavelengths (26 to

190 nm) and skyrmion diameters (9 to 74 nm). The deflection angle, θ, is defined as the angle between the forward-moving wave front (in the x direction) and the deflected wave front. There are two clearly distinguishable regimes: For small ratios (magnon wavelength smaller than the skyrmion diameter), the deflection angle increases with R, until a maximum of nearly 30˚ is reached when the magnon wavelength and skyrmion diameter are comparable in size ($R \approx 1$). This maximum value is consistent with previous theoretical studies of magnon-skyrmion interactions [36,37]. The inset in Fig. 2 shows an example of a spin wave deflection pattern with a deflection angle of approximately 27˚. As the magnon wavelength becomes larger than the skyrmion diameter, the deflection angle reduces again. This is expected since the longer waves are less perturbed by the skyrmion, and no deflection is expected in the limit of $R \rightarrow \infty$.

It is worth noting that the interaction between magnetic bubbles and propagating spin waves has also been analytically studied in a recent work [52], where it was shown to only result in a "side jump" of the spin wave passing through the magnetic texture. A spin wave deflection with a finite angle, on the other hand, was shown to necessarily require the presence of a topologically non-trivial skyrmion, consistent with the results presented here.

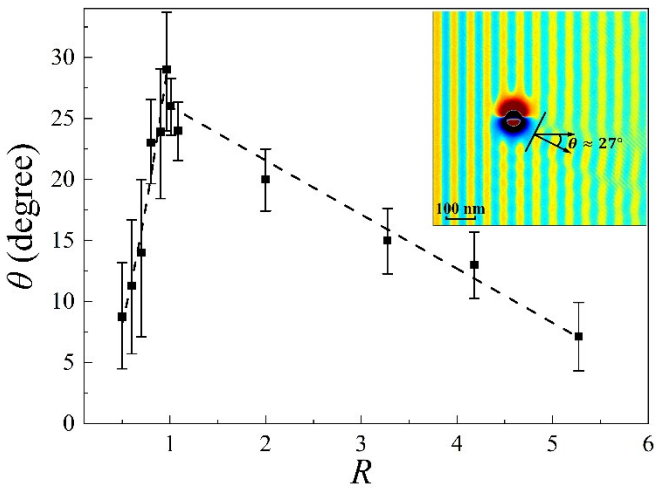

FIG 2. Magnon deflection angle (θ) as a function of the ratio of magnon wavelength to skyrmion diameter (R). The deflection angle is maximized when the wavelength and skyrmion diameter are comparable. The inset shows a simulated spin wave deflection pattern with deflection angle of 27° at $R \approx 1$, corresponding to the case of K_u = 0.36 MJ m^{-3} and D = 1.7 mJ m^{-2}.

This result indicates the possibility to manipulate the magnon deflection angle by tuning the ratio of magnon wavelength to skyrmion diameter. This can be achieved by either the manipulation of the skyrmion size or magnon wavelength through electrical control of the i-DMI and PMA coefficients, according to the equations given in the caption of Fig. 1. While it is in principle possible to tune the i-DMI by external signals such as electric fields [53] or strain [53,54], here we focus on the control of the perpendicular magnetic anisotropy, which can be modified by applying moderate voltages via the interfacial VCMA effect [40,42-44]. To do so, a voltage gate can be constructed on top of the ferromagnet using a thin dielectric layer (e.g. MgO) as the gate oxide. In this way, two types of gating are in principle possible: (i) A local voltage can be applied only in the skyrmion region of the device to effectively manipulate the skyrmion size, while leaving the PMA (and hence spin wave dispersion) unchanged outside the gate region. Such a local voltage gate can also create a pinning potential for the skyrmion due to the resulting anisotropy gradient at the gate edges [31,55], preventing the movement of the skyrmion. (ii) A global electric field can be applied to the entire structure, controlling both the skyrmion diameter and the magnon wavelength at the same time. This method has the advantage of avoiding unwanted spin wave reflections due to the anisotropy gradients induced by a local gate. It also realizes a large manipulation of R with a relatively narrow range of gate voltages, since both magnon wavelength and skyrmion diameter are changed simultaneously by the applied voltage. In what follows, we will therefore primarily focus on this second scenario.

B. Voltage-controlled skyrmionic magnon switch

We simulated the latter scenario by varying the global PMA coefficient while keeping the other simulation parameters constant and measuring the deflection angle of the spin waves in the magnetic wire as a function of the PMA. The results are summarized in Fig. 3, which indicates a reduction of the deflection angle with increasing anisotropy constant over the range of PMA values that were studied. The results can be explained in terms of the PMA-induced modification of the skyrmion diameter and magnon wavelength. Specifically, larger PMA values reduce the skyrmion size (see Fig. 1(b))

while increasing the magnon wavelength for a given frequency, thus increasing R and pushing the deflection angle to lower values, as expected from Fig. 2. Note that the leftmost data point of Fig. 3 (showing the magnon deflection angle with a uniaxial PMA constant of K_u = 0.36 MJ m^{-3}) corresponds to $R \approx 1$, i.e., the maximum deflection angle shown in Fig. 2. The corresponding spin wave front is shown in the inset of Fig. 2.

A linear fit to the data in Fig. 3 indicates a change of the deflection angle of $d\theta/dK_u \approx 0.25^{\circ}$/(kJ m^{-3}), which, assuming a magnetic film thickness of 1 nm and an entirely interfacial origin of the PMA, translates to $d\theta/dK_i \approx 0.25^{\circ}$/(μJ m^{-2}), where K_i is the interfacial anisotropy energy density [56]. Assuming the modification of the anisotropy, in turn, is occurring via the interfacial VCMA effect with a typical VCMA coefficient of 100 fJ/Vm [42,44], this translates to a deflection angle of $d\theta/dE_{gate} \approx 25^{\circ}$/(V nm^{-1}), where E_{gate} is the electric field applied across the gate oxide. Thus, for an oxide thickness of ~ 1 nm (similar to a typical VCMA-controlled magnetic tunnel junction), the deflection angle can be electrically controlled over a wide range up to ~ 30° using a fairly low voltage of 1 V. Increasing the VCMA coefficient will further reduce the gate voltage required for electrical control of the magnon deflection angle.

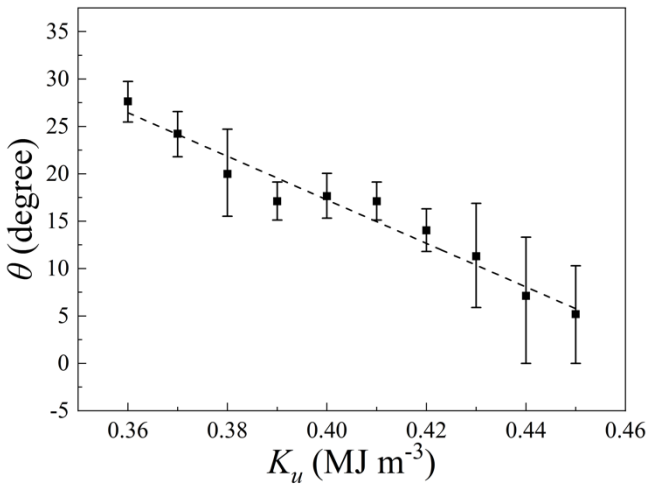

FIG 3. (a) Dependence of the deflection angle (θ) on the PMA coefficient (K_u) for D = 1.7 mJ m^{-2}. The spin wave frequency is f = 30 GHz, with wavelengths varying from 60 nm to 180 nm depending on the anisotropy. Simulations considering the opposite skyrmion polarity (not shown) resulted in the same range of deflection angles, but with an opposite sign, i.e., indicating deflection in the opposite direction.

Based on these results, we next investigate a skyrmionic magnon switch device, which

can provide voltage-controlled routing of spin waves in a network of magnetic wires. The device uses a magnonic waveguide similar to the previous simulations, with a branch connected at an angle (30° in the following simulations), as shown in Fig. 4(a). The principal dimensions of the ferromagnetic layer of the SMS (with thickness of 1 nm) are shown in this figure. The i-DMI coefficient was set to 1.7 mJ m^{-2}. All other material parameters were the same as in the previous simulations, except the anisotropy constant (K_u), which was varied to control the skyrmion diameter (hence R), thus simulating the VCMA effect. In all cases, the skyrmion position was set at the cross point of the center line of the branch and a horizontal line with a distance of 100 nm from the lower edge of the main track.

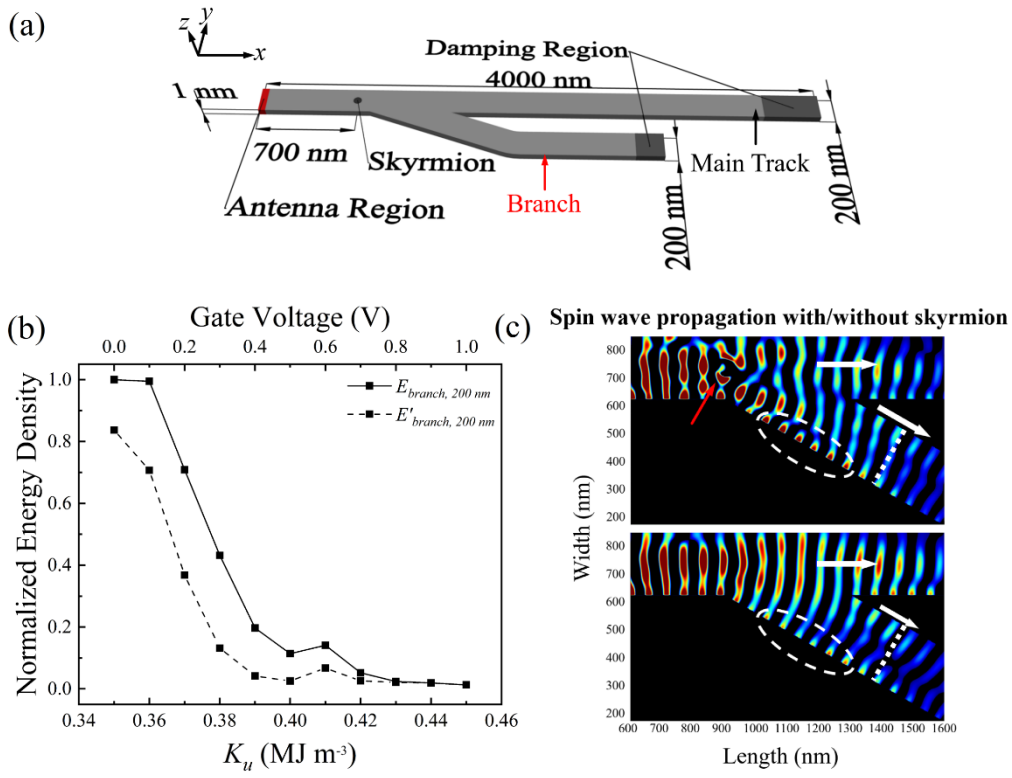

FIG 4. (a) Schematic of the SMS device. (b) Dependence of the normalized spin wave energy density in the branch on K_u. E_{branch} and E'_{branch} represent the normalized energy density in the branch, in the cases with and without a skyrmion, respectively. (c) Simulated spin wave propagation pattern in cases with or without a skyrmion. The skyrmion diameter is ~30 nm for K_u = 0.36 MJ m^{-3}. White arrows show the spin wave propagation direction. The red arrow indicates the position of the skyrmion. White circles demonstrate the edge mode spin wave. The white dotted line indicates the position where the spin wave energy density was measured.

We characterize the efficiency of the magnon routing in the proposed device by comparing the normalized energy density of spin waves in the branch as a function of K_u, in the cases with a skyrmion at the intersection (E), and without a skyrmion (E'), as shown in Fig. 4(b). The energy density is always measured at the same position in the branch, at a distance of 700 nm from the skyrmion, and normalized to the maximum energy density (i.e. the case with a skyrmion, main track width of 200 nm, and K_u of 0.35 MJ m^{-3}). The energy density is calculated from $E = (1/S)\int \boldsymbol{m}^2 dS$, where S is the integral area defined as the wavelength multiplied by the width of the branch, and $\boldsymbol{m}$ is the ac magnetization. The results show a maximum of the normalized energy density in the branch for K_u = 0.35 MJ m^{-3}.

A critical parameter for the SMS device is its on/off ratio, which we define here as the ratio of the spin wave energy densities in the SMS branch when the device is "on" (i.e., the energy density in the branch is maximized) to when it is "off" (i.e., the energy density in the branch is minimized). This ratio is limited by at least two factors. First, note that skyrmion will asymmetrically scatter the spin wave. Part of the spin wave always continues to propagate in the main track for typical skyrmion sizes that were considered here, which were small compared to the overall track width. This limits the maximum power that can be deflected into the branch, thus limiting the on/off ratio. Second, a finite spin wave energy can be observed in the branch even with large K_u values (small skyrmions and deflection angle) or in the absence of a skyrmion. As shown in Fig 4(b), $E'_{branch,\ 200\ nm}$ represents the normalized energy density in the branch in the case without a skyrmion, which can reach ~ 80% of the maximum of the branch energy density in the case with a skyrmion at a K_u value of 0.35 MJ m^{-3}. The first reason for this is that the finite width of the waveguide (main track) results in edge reflections that drive part of the wave into the branch, irrespective of the presence or absence of the skyrmion. In addition, as observed in Fig. 4(c), there are spin waves that propagate regardless of the skyrmion presence or waveguide width, and are localized near the wire edges due to the laterally nonuniform effective magnetic field inside the wire [57,58]. These edge mode spin waves increase the minimum achievable spin wave energy in the

off state of the device, thus again limiting the on/off ratio.

To solve this problem, we compared different lateral widths of the main track while keeping the branch width unchanged. In this new configuration, the spin wave front in the main track is closer to that of a uniform plane wave, resulting in a smaller edge reflection of the wave into the branch in the absence of a skyrmion (hence reducing the off-state spin wave energy in the branch).

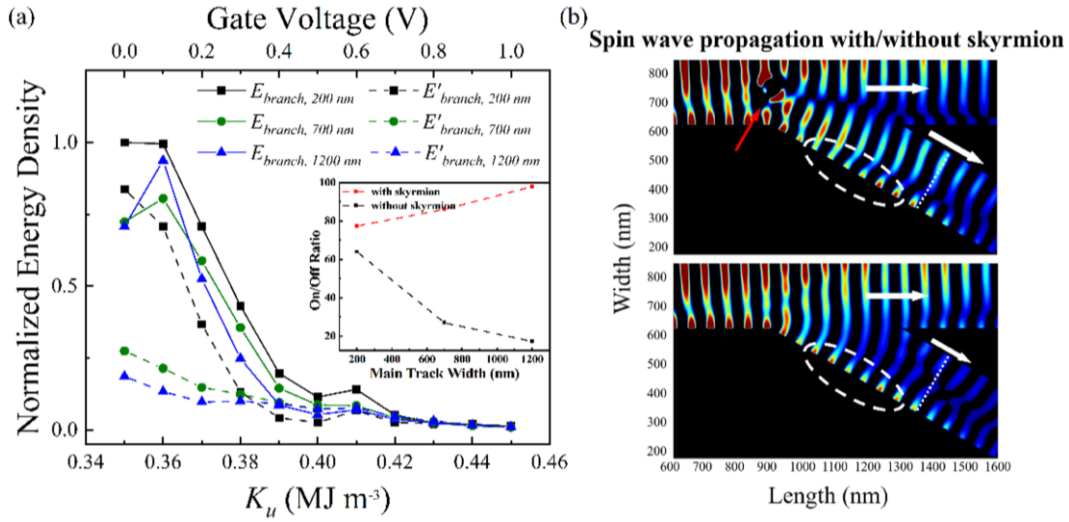

FIG 5. (a) Dependence of normalized energy density in the branch on both K_u and gate voltage with different main track widths. E_{branch} and E'_{branch} represent the normalized energy density in the branch with and without the skyrmion, respectively. The inset compares the on/off ratio for the cases with and without the skyrmion, as a function of the main track width. (b) Simulated spin wave propagation in the cases with and without a skyrmion. The skyrmion diameter is ~30 nm for K_u = 0.36 MJ m^{-3}. Only part of the track is shown in this figure. The main track width is 1200 nm. White arrows show the spin wave propagation. Red arrow indicates the skyrmion. White circles indicate the edge mode spin wave. Note the apparent nonreciprocity of the edge mode, which is a consequence of DMI as reported previously [59]. The white dotted line indicates the position where the spin wave energy density was measured.

The simulated waveforms for the case with main track width of 1200 nm are shown in Fig. 5(b), where the white arrows show the propagation direction of the spin wave front, while the red arrow indicates the location of the skyrmion. With this wider main track, unlike the previous case of Fig. 4, the energy density in the branch in the case without skyrmion is much lower than in the case with a skyrmion. Thus, increasing the width of the main track reduces the magnons entering the branch and thereby decreases the minimum achievable spin wave energy in the off state of the device, thus increasing

its on/off ratio. Figure 5(a) shows the normalized energy density as a function of K_u, in cases with and without the skyrmion, for different widths of the main track, clearly demonstrating this trend. The subplot in Fig 5(a) shows the dependence of on/off ratio on the main track. The on/off ratio can be as large as 90× with a main track width of 1200 nm, which is an increase by ~ 40% compared with the case of 200 nm width. It is worth noting that in the case with the skyrmion, for wider main tracks (700 and 1200 nm), the normalized energy density will reach its maximum at K_u of 0.36 MJ m^{-3}. This is the PMA value where the deflection angle is close to 30˚ according to our previous results (Fig. 3), which also matches well with the angle between the main track and the branch (30˚). Therefore, most of the deflected magnons can enter the branch, leading to a maximum of the normalized energy density.

It is worth noting, however, that even for such a wide waveguide (1200 nm), the normalized energy density in the branch in the absence of the skyrmion is not zero, limiting the on/off ratio. This finite off-state energy density is largely a result of the remaining edge mode spin waves (highlighted in Fig. 5(b)). Therefore, while on/off ratios even higher than 90× are in principle possible in an optimized SMS device geometry, the achievable on/off ratio will ultimately be limited by the presence of these edge modes.

Additional simulations were performed with different branch angles, to test the influence of the angle on the on/off ratio. The results are shown in Fig. 6. From this figure, it is observed that having either a larger or smaller branch angle deviating from 30˚ will reduce the on/off ratio. This is as expected, since the maximum spin wave deflection angle (when the ratio of wavelength to skyrmion diameter is ~ 1) coincides with this value. Nonetheless, the on/off ratio is quite large (~85) even in the case of a 40˚ branch angle, which can be useful in applications.

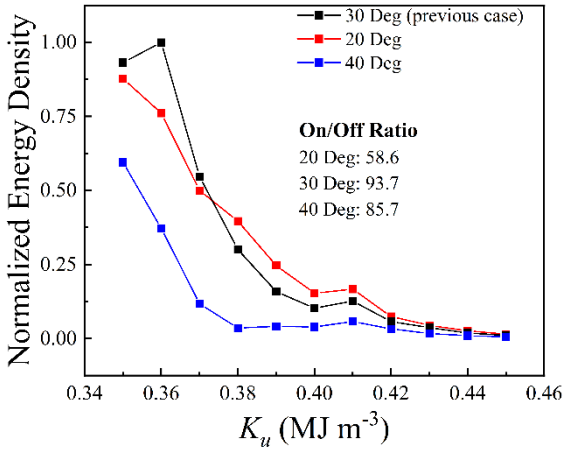

FIG 6. Normalized energy density in the branch as a function of Ku values for different branch angles. The maximum values of the on/off ratio for different branch angles are also shown in the figure.

Finally, we repeated the simulations considering a gate localized only to the skyrmion area, while considering a main track width of 1200 nm and branch width of 200 nm. The results are shown in Fig. 7. As expected, the on/off ratio is significantly lower than the case with global VCMA, since only the local interaction between the skyrmion and spin wave plays a role in the on/off ratio in this case, resulting in a maximum ratio close to ~ 4. On the other hand, it is noteworthy that in the case without the skyrmion, the energy density in the branch is nearly independent of the anisotropy (hence gating electric field), as expected. This confirms that in the case of local VCMA gating, the presence of the skyrmion is essential for the operation of the SMS device.

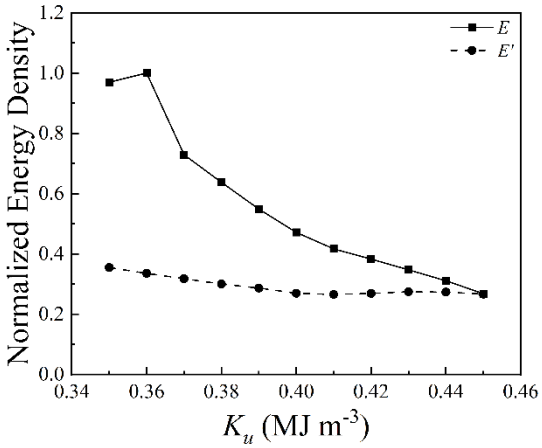

FIG 7. Normalized energy density in the branch as a function of K_u values for the case with local VCMA gating. All material parameters are the same as the case of global VCMA gating, with branch width of 200 nm and main track width of 1200 nm. *E* and *E'* represent the normalized energy density in the branch with and without the skyrmion, respectively.

It is worth noting that, in terms of practical implementation, the exchange spin waves considered here are more difficult to excite than dipole spin waves with longer wavelengths. However, we focused on the short-wavelength exchange-dominated regime mainly for three reasons: (i) As shown in Fig. 2, increasing the ratio of magnon wavelength to skyrmion diameter reduces the spin wave deflection, with the deflection becoming nearly zero when R is ~7 or larger. (ii) Magnetostatic spin wave modes with longer wavelengths are unable to efficiently propagate through narrow magnetic waveguides. (iii) Short exchange spin waves lead to overall smaller magnonic devices, which is an important requirement for computing applications, where a large number of such devices have to be placed relatively close together.

In addition, it is possible to imagine device structures that utilize electric-field-dependent effects other than VCMA to manipulate either skyrmion properties or magnon dispersion, thus allowing for voltage-controlled SMS operation based on alternative mechanisms. One example is the electric field control of DMI, which has been studied in recent reports [60,61].

III. Conclusions

In summary, this work micromagnetically demonstrated the manipulation of the spin wave propagation direction using a Néel skyrmion as a voltage-controlled scattering center. The spin wave deflection angle can be electrically controlled over a wide range up to ~30˚ via the VCMA effect, using experimentally realistic material parameters and a gate voltage less than 1 V. Using this voltage-controlled deflection, we proposed and analyzed a skyrmionic magnon switch, which provides an on/off ratio of up to 90× within the range of material parameters considered in this work. The SMS may serve as an electrically programmable magnon switch for routing spin waves in emerging magnonic computing circuits.

Acknowledgements

This work was in part supported by the National Science Foundation Materials Research Science and Engineering Center at Northwestern University (NSF DMR-1720319), and in part by a grant from the National Science Foundation, Division of Industrial Innovation and Partnerships (NSF IIP-1919109). The authors thank Prof. Pramey Upadhyaya (Purdue University) for helpful discussions.

References:

[1] M. P. Kostylev, A. A. Serga, T. Schneider, B. Leven, and B. Hillebrands, Spin-wave logical gates, Applied Physics Letters **87**, 153501 (2005).

[2] T. Schneider, A. A. Serga, B. Leven, B. Hillebrands, R. L. Stamps, and M. P. Kostylev, Realization of spin-wave logic gates, Applied Physics Letters **92**, 022505 (2008).

[3] A. Khitun, M. Bao, and K. L. Wang, Magnonic logic circuits, Journal of Physics D: Applied Physics **43**, 264005 (2010).

[4] P. Shabadi, S. N. Rajapandian, S. Khasanvis, and C. A. Moritz, Design of spin wave functions-based logic circuits, Spin **2**, 1240006 (2012).

[5] P. Khalili and K. L. Wang, The computer chip that never forgets, IEEE Spectrum **52**, 30 (2015).

[6] A. Khitun, D. E. Nikonov, and K. L. Wang, Magnetoelectric spin wave amplifier for spin wave logic circuits, Journal of Applied Physics **106**, 123909 (2009).

[7] K. Wang and P. K. Amiri, Nonvolatile spintronics: perspectives on instant-on nonvolatile nanoelectronic systems, Spin **2**, 1250009 (2012).

[8] S. Cherepov *et al.*, Electric-field-induced spin wave generation using multiferroic magnetoelectric cells, Applied Physics Letters **104**, 082403 (2014).

[9] S. Dutta, S.-C. Chang, N. Kani, D. E. Nikonov, S. Manipatruni, I. A. Young, and A. Naeemi, Non-volatile clocked spin wave interconnect for beyond-CMOS nanomagnet pipelines, Scientific reports **5**, 9861 (2015).

[10] A. Kozhevnikov, F. Gertz, G. Dudko, Y. Filimonov, and A. Khitun, Pattern recognition with magnonic holographic memory device, Applied Physics Letters **106**, 142409 (2015).

[11] M. Balynsky, D. Gutierrez, H. Chiang, A. Khitun, A. Kozhevnikov, Y. Khivintsev, G. Dudko, and

Y. Filimonov, Parallel Data Processing With Magnonic Holographic Co-Processor, in *2016 IEEE International Conference on Rebooting Computing (ICRC)* (IEEE, 2016), pp. 1.

[12] X. Zhang, C.-L. Zou, L. Jiang, and H. X. Tang, Strongly coupled magnons and cavity microwave photons, Physical review letters **113**, 156401 (2014).

[13] X. Zhang, N. Zhu, C.-L. Zou, and H. X. Tang, Optomagnonic whispering gallery microresonators, Physical review letters **117**, 123605 (2016).

[14] D. Lachance-Quirion, Y. Tabuchi, A. Gloppe, K. Usami, and Y. Nakamura, Hybrid quantum systems based on magnonics, Applied Physics Express **12**, 070101 (2019).

[15] N. Lauk, N. Sinclair, S. Barzanjeh, J. P. Covey, M. Saffman, M. Spiropulu, and C. Simon, Perspectives on quantum transduction, Quantum Science Technology **5**, 020501 (2020).

[16] K. Vogt, H. Schultheiss, S. Jain, J. Pearson, A. Hoffmann, S. Bader, and B. Hillebrands, Spin waves turning a corner, Applied Physics Letters **101**, 042410 (2012).

[17] Q. Wang, P. Pirro, R. Verba, A. Slavin, B. Hillebrands, and V. Chumak Andrii, Reconfigurable nanoscale spin-wave directional coupler, Science Advances **4**, e1701517 (2018).

[18] Q. Wang *et al.*, A magnonic directional coupler for integrated magnonic half-adders, Nature Electronics **3**, 765 (2020).

[19] X.-g. Wang, G.-h. Guo, and J. Berakdar, Steering magnonic dynamics and permeability at exceptional points in a parity–time symmetric waveguide, Nature Communications **11**, 5663 (2020).

[20] X.-G. Wang, G.-H. Guo, and J. Berakdar, Electric steering of spin excitation in nanostructured synthetic antiferromagnet, Applied Physics Letters **117**, 242406 (2020).

[21] X.-g. Wang, G.-h. Guo, and J. Berakdar, Enhanced Sensitivity at Magnetic High-Order Exceptional Points and Topological Energy Transfer in Magnonic Planar Waveguides, Physical Review Applied **15**,

034050 (2021).

[22] A. Fert, N. Reyren, and V. Cros, Magnetic skyrmions: advances in physics and potential applications, Nature Reviews Materials **2**, 1 (2017).

[23] A. Chacon *et al.*, Observation of two independent skyrmion phases in a chiral magnetic material, Nature Physics **14**, 936 (2018).

[24] S. Woo *et al.*, Observation of room-temperature magnetic skyrmions and their current-driven dynamics in ultrathin metallic ferromagnets, Nature materials **15**, 501 (2016).

[25] S. D. Pollard, J. A. Garlow, J. Yu, Z. Wang, Y. Zhu, and H. Yang, Observation of stable Néel skyrmions in cobalt/palladium multilayers with Lorentz transmission electron microscopy, Nature communications **8**, 1 (2017).

[26] W. Jiang *et al.*, Direct observation of the skyrmion Hall effect, Nature Physics **13**, 162 (2017).

[27] A. Fert, V. Cros, and J. Sampaio, Skyrmions on the track, Nature nanotechnology **8**, 152 (2013).

[28] J. Sampaio, V. Cros, S. Rohart, A. Thiaville, and A. Fert, Nucleation, stability and current-induced motion of isolated magnetic skyrmions in nanostructures, Nature nanotechnology **8**, 839 (2013).

[29] G. Yu *et al.*, Room-temperature skyrmion shift device for memory application, Nano letters **17**, 261 (2017).

[30] W. Jiang *et al.*, Blowing magnetic skyrmion bubbles, Science **349**, 283 (2015).

[31] P. Upadhyaya, G. Yu, P. K. Amiri, and K. L. Wang, Electric-field guiding of magnetic skyrmions, Physical Review B **92**, 134411 (2015).

[32] D. Bhattacharya, S. A. Razavi, H. Wu, B. Dai, K. L. Wang, and J. Atulasimha, Creation and annihilation of non-volatile fixed magnetic skyrmions using voltage control of magnetic anisotropy, Nature Electronics, 1 (2020).

[33] K. Everschor, M. Garst, B. Binz, F. Jonietz, S. Mühlbauer, C. Pfleiderer, and A. Rosch, Rotating skyrmion lattices by spin torques and field or temperature gradients, Physical Review B **86**, 054432 (2012).

[34] X. Zhang, M. Ezawa, D. Xiao, G. Zhao, Y. Liu, and Y. Zhou, All-magnetic control of skyrmions in nanowires by a spin wave, Nanotechnology **26**, 225701 (2015).

[35] M. Shen, Y. Zhang, J. Ou-Yang, X. Yang, and L. You, Motion of a skyrmionium driven by spin wave, **112**, 062403 (2018).

[36] J. Iwasaki, A. J. Beekman, and N. Nagaosa, Theory of magnon-skyrmion scattering in chiral magnets, Physical Review B **89**, 064412 (2014).

[37] C. Schütte and M. Garst, Magnon-skyrmion scattering in chiral magnets, Physical Review B **90**, 094423 (2014).

[38] S. Schroeter and M. Garst, Scattering of high-energy magnons off a magnetic skyrmion, Low Temperature Physics **41**, 817 (2015).

[39] K.-W. Moon, B. S. Chun, W. Kim, and C. Hwang, Control of spin-wave refraction using arrays of skyrmions, Physical Review Applied **6**, 064027 (2016).

[40] T. Maruyama *et al.*, Large voltage-induced magnetic anisotropy change in a few atomic layers of iron, Nature nanotechnology **4**, 158 (2009).

[41] X. Li *et al.*, Enhancement of voltage-controlled magnetic anisotropy through precise control of Mg insertion thickness at CoFeB| MgO interface, Applied Physics Letters **110**, 052401 (2017).

[42] P. K. Amiri and K. L. Wang, Voltage-controlled magnetic anisotropy in spintronic devices, Spin **3**, 1240002 (2012).

[43] Z. Wen, H. Sukegawa, T. Seki, T. Kubota, K. Takanashi, and S. Mitani, Voltage control of magnetic

anisotropy in epitaxial Ru/Co 2 FeAl/MgO heterostructures, Scientific reports **7**, 45026 (2017).

[44] T. Nozaki, T. Yamamoto, S. Miwa, M. Tsujikawa, M. Shirai, S. Yuasa, and Y. Suzuki, Recent progress in the voltage-controlled magnetic anisotropy effect and the challenges faced in developing voltage-torque MRAM, Micromachines **10**, 327 (2019).

[45] A. Vansteenkiste and B. Van de Wiele, MuMax: A new high-performance micromagnetic simulation tool, Journal of Magnetism Magnetic Materials **323**, 2585 (2011).

[46] A. Vansteenkiste, J. Leliaert, M. Dvornik, M. Helsen, F. Garcia-Sanchez, and B. V. Waeyenberge, The design and verification of MuMax3, AIP Advances **4**, 107133 (2014).

[47] G. Consolo, L. Lopez-Diaz, L. Torres, and B. Azzerboni, Boundary conditions for spin-wave absorption based on different site-dependent damping functions, IEEE transactions on magnetics **43**, 2974 (2007).

[48] G. Venkat, M. Franchin, H. Fangohr, and A. Prabhakar, Mesh Size and Damped Edge Effects in Micromagnetic Spin Wave Simulation, arXiv preprint (2014).

[49] X. Wang, H. Yuan, and X. Wang, A theory on skyrmion size, Communications Physics **1**, 1 (2018).

[50] H. Hata, T. Moriyama, K. Tanabe, K. Kobayashi, R. Matsumoto, S. Murakami, J.-i. Ohe, D. Chiba, and T. Ono, Micromagnetic simulation of spin wave propagation in a ferromagnetic film with different thicknesses, Journal of the Magnetics Society of Japan, 1506R004 (2015).

[51] S. Bance, T. Schrefl, G. Hrkac, A. Goncharov, D. A. Allwood, and J. Dean, Micromagnetic calculation of spin wave propagation for magnetologic devices, Journal of Applied Physics **103**, 07E735 (2008).

[52] J. Lan and J. Xiao, Skew scattering and side jump of spin wave across magnetic texture, Physical Review B **103**, 054428 (2021).

[53] T. Koyama, Y. Nakatani, J. i. Ieda, and D. Chiba, Electric field control of magnetic domain wall motion via modulation of the Dzyaloshinskii-Moriya interaction, Science advances **4**, eaav0265 (2018).

[54] N. Gusev, A. Sadovnikov, S. Nikitov, M. Sapozhnikov, and O. Udalov, Manipulation of the Dzyaloshinskii–Moriya Interaction in Co/Pt Multilayers with Strain, Physical Review Letters **124**, 157202 (2020).

[55] Y. Zhou, R. Mansell, and S. van Dijken, Driven gyrotropic skyrmion motion through steps in magnetic anisotropy, Scientific reports **9**, 1 (2019).

[56] S. Ikeda *et al.*, A perpendicular-anisotropy CoFeB–MgO magnetic tunnel junction, Nature materials **9**, 721 (2010).

[57] J. Park, P. Eames, D. Engebretson, J. Berezovsky, and P. Crowell, Spatially resolved dynamics of localized spin-wave modes in ferromagnetic wires, Physical review letters **89**, 277201 (2002).

[58] A. Lara, J. R. Moreno, K. Y. Guslienko, and F. G. Aliev, Information processing in patterned magnetic nanostructures with edge spin waves, Scientific reports **7**, 1 (2017).

[59] F. Garcia-Sanchez, P. Borys, A. Vansteenkiste, J.-V. Kim, and R. L. Stamps, Nonreciprocal spin-wave channeling along textures driven by the Dzyaloshinskii-Moriya interaction, Physical Review B **89**, 224408 (2014).

[60] X.-g. Wang, L. Chotorlishvili, G.-h. Guo, and J. Berakdar, High-Fidelity Magnonic Gates for Surface Spin Waves, Physical Review Applied **12**, 034015 (2019).

[61] X. G. Wang, L. Chotorlishvili, N. Arnold, V. K. Dugaev, I. Maznichenko, J. Barnaś, P. A. Buczek, S. S. P. Parkin, and A. Ernst, Plasmonic Skyrmion Lattice Based on the Magnetoelectric Effect, Physical Review Letters **125**, 227201 (2020).